ChemPhysChem

Research Article
doi.org/10.1002/cphc.202400370

Chemistry Europe
European Chemical Societies Publishing

www.chemphyschem.org

On the Relationship between Water Adsorption and Surface Chemistry in Soda-lime Silicate Glasses

Achraf Atila*[a]

Understanding how the surface structure affects the bioactivity and degradation rate of the glass is one of the primary challenges in developing new bioactive materials. Here, classical and reactive molecular dynamics simulations are used to investigate the relationship between local surface chemistry and local adsorption energies of water on three soda-lime silicate glasses. The compositions of the glasses, $(SiO_2)_{65-x}$-$(CaO)_{35}(Na_2O)_x$ with $x = 5$, 10, and 15, were chosen for their bioactive properties. Analysis of the glass surface structure, compared to the bulk structure, showed that the surface is rich in modifiers and non-bridging oxygen atoms, which were correlated with local adsorption energies. The reactivity of the glasses is found to increase with higher Na_2O content, attributed to elevated Na cations and undercoordinated species at the glass surfaces. The current work provides insights into the relationship between the surface structure, chemistry, and properties in these bioactive glasses and offers a step toward their rational design.

Introduction

Historically, biomaterials were chosen to be as inert as possible. However, in the last decades, it became more prominent to use biologically active "bioactive" materials to evoke a targeted biological response,[1–3] which is a result of the formation of a bond between the tissues and the material.[2–5] Such examples of materials are oxide glasses, which were used as bioactive materials with applications in many medical fields. This includes curing cancerous cells by increasing the acidity of the environment locally, achieved by having a controlled ion release.[6] In addition to that, they found applications in restorative and regenerative biomedical applications such as orthopedic, dental, maxillofacial implants, and tissue engineering.[3] Bioactive glasses are favored among other alternatives due to their ability to degrade in the body over time, allowing the possibility to control the ion release and to enable bone regeneration instead of replacement, leading to a restoration of the original bone state and function.[7]

The first interaction between the biological tissue and the bioactive glass happens at the interface between the glass and the tissue.[8] In the case of water, the water molecules chemisorb on the glass surface, and the hydroxyl groups are formed on the surface that becomes hydroxylated.[8,9] The change in the properties of the hydroxylated glass surfaces[10] compared to the dry glass surface is because the hydroxyl groups bonded to the surface make it more stable than having only dangling bonds. Contact between water and an oxide glass surface generally leads to the depolymerization of the glass network by breaking Si–O–Si bonds and forming silanol groups (Si–O–H). This process results from forming new hydroxyl groups (OH) due to the dissociation of water molecules.[8,9] On the other side, the bioactivity of glasses comes from their ability to form hydroxycarbonate apatite (HCA, $Ca_{10}(PO_4)_{6-y}(CO_3)_y(OH)_{2-y}$, with y being the CO_3 content[11,12]) on the surface, bonding to the bones, release ions, and, more importantly, degrade in the body.[13–16] Thus, understanding the surface properties of oxide glasses and linking the surface chemistry to bioactivity is paramount.

There are only a few molecular dynamics (MD) simulation studies on the adsorption of water on silicate glass surfaces that tried to link the surface structure and reactivity. For instance, Bakaev and Steele[17] demonstrated that defects in the atomic structure of vitreous silica, such as single or triple coordinated oxygen atoms and distorted SiO_4 tetrahedra, create stronger electrostatic fields compared to defect-free surfaces, enhancing surface hydrophilicity by interacting with water molecules. These findings contradict the expectation that surfaces devoid of hydroxyl groups are hydrophobic, suggesting that atomic structures of silica surfaces vary depending on their formation process. In another study, Leed and Pantano[18] studied the water adsorption on silica and silicate glass fracture surfaces using MD simulations. Their conclusion suggests that the strongest adsorption sites are linked to defects within the network rather than modifier species, which, although introducing water adsorption sites, are comparatively weaker than those associated with network defects.

Recently, Yu et al.[19] conducted a study using reactive molecular dynamics to investigate the relationship between topological constraints and surface energy, explicitly focusing on the transition from hydrophilic to hydrophobic behavior on silica surfaces. They showed that silica exhibits a hydrophilic-to-hydrophobic transition that is controlled by the atomic topology of its surface. Wilkinson et al.[20] used reactive MD simulations and density functional theory to study the effect of

[a] A. Atila
Department of Material Science and Engineering, Saarland University, Saarbrücken, 66123, Germany
E-mail: achraf.atila@uni-saarland.de

glass network topology on the surface reactivity of glasses, which evidenced the existence of a chemically stable intermediate phase on the surface of the glass where the glass network is mechanically isostatic.

Here, using classical and reactive MD simulations, we present a detailed study of the effect of glass composition on the surface structure and water adsorption of recently developed bioactive soda-lime silicate glasses.[8] The soda-lime silicate glasses are made of silica (SiO_2), sodium oxide (Na_2O), and calcium oxide (CaO), with the possibility of containing traces of magnesium oxide and alumina.[21] These glasses exhibit better mechanical performance and chemical durability than the reference glass in this field, the 45S5 bioactive glass.[15,21,22] They also have a structure that makes them highly bioactive in physiological environments.[8] Upon interaction with body fluids, the glass releases modifier ions, such as Na and Ca, leading to the dissolution of the silica network and the formation of a silica-rich gel layer on the glass surface. This layer attracts calcium and phosphate ions from the surrounding fluids, resulting in the precipitation and subsequent crystallization of HCA. The formation of HCA is vital as it enhances osteoconductivity, allowing for the attachment and growth of bone-forming cells, and enables a strong chemical bond with natural bone tissue.[22]

Bulk glasses and melt surfaces are prepared using a combination of classical MD and reactive MD simulations. Local adsorption energy maps at 300 K are obtained and correlated to the surface structure and chemistry. Finally, we provide an atomistic understanding by an attempt to link the observed change to the bioactive nature of these glasses.

Methods

Glass Preparation

The SHIK potential[23] was used to model the interactions between the atoms and prepare the initial glass configurations. In this model, the atoms are treated as fixed charged points, with the charge of oxygen being composition-dependent, interacting via short-range Buckingham potential and long-range Coulomb interactions. An additional repulsive r^{-24} therm is added to properly treat the interactions at high temperature and pressure.[23] The short-range cutoff was set to 8.0 Å, and the long-range interactions were solved using the damped-shifted-force model[24] with 0.2 $Å^{-1}$ as a damping coefficient and 10.0 Å, as a long-range cutoff. Potential parameters and partial charges can be found in Ref. [23].

The soda-lime silicate glasses of the following composition $(SiO_2)_{65-x}(CaO)_{35}(Na_2O)_x$ with x = 5, 10, and 15 were prepared by the melt-quenching technique, which is often used for the preparation of bulk glasses in atomistic simulations.[14,25–31] Initially, 10600 atoms were inserted randomly in a cubic simulation box with periodicity imposed in all directions. Unless otherwise stated, the time step was set to 1 fs in all simulations. The samples were equilibrated at a high temperature (T = 4000 K) in the canonical ensemble (NVT constant number of atoms, volume, and temperature) for 300 ps. Then, the system was further equilibrated in the NPT ensemble (constant number of atoms, pressure, and temperature) for 700 ps at the same temperature with an imposed external pressure of 100 MPa, which was ramped to 0 MPa during the cooling. The equilibrated liquids were quenched from 4000 K to 300 K using a cooling rate of 1 K/ps. A production run in the canonical ensemble at 300 K for 100 ps was performed to statistically average the structural properties. All simulations are performed using LAMMPS code,[32] and all atomic visualizations are done using OVITO.[33] The density and glass transition temperature T_g of all compositions are reported in Table 1.

Surface Preparation

The surface of the glasses was prepared by relaxing a configuration at 2300 K, which is $\approx 1.3T_g$ using periodic boundary conditions in all spacial directions for 100 ps. Then, a surface was created by adding a vacuum of 10 Å along the *z*-axis at the top and bottom. The surface was equilibrated for 500 ps at the same temperature (2300 K). Afterward, a quenching to 300 K was performed using 1 K/ps as a cooling rate. At 300 K the temperature was further relaxed for 1000 ps. The glasses with the surfaces were subjected to an equilibration at 300 K for 250 ps using the reactive force field ReaxFF,[34] with the parametrization from Senftle et al.[35] During the ReaxFF simulations, the timestep was reduced to 0.25 fs, and the charge equilibration was performed for every 100 timesteps using the Qeq formalism.[36–38] The choice of the charge equilibrating frequency is based on the fact that at low temperatures (300 K), the diffusion of the atoms is very low, and the atoms do not change their environment very frequently. Moreover, different charge equilibrating frequencies were checked for the robustness of the results.

Adsorption Energy Calculation

The calculation of the adsorption energy or, also known as the binding energy, E_{ads} was obtained using the ReaxFF[34] force field at a temperature of 300 K using eq. 1.

$$E_{ads} = E_{GW} - (E_G + E_W), \quad (1)$$

where E_{GW}, E_G, and E_W are the potential energies of the glass with the water molecule on its surface, the potential energy of the glass surface without a water molecule, and the potential energy of a free water molecule in the gas phase, respectively. The upper surface of the glasses was divided into 50×50 grid, resulting in 2500 grid points for each glass surface. A single water molecule was used to scan the grid and determine the local adsorption energy as schematically depicted in Figure 1 while allowing for potential chemical reactions between the water molecule and the glass surface. The water molecule is added for each grid pixel with a separation distance of 3 Å from the surface. The position of the center of mass of the water molecule was constrained in the *x*- and *y*-direction in a way to keep it fixed at that (*x*,*y*)-coordinates, while the *z*-position was allowed to move freely. The hydrogen atoms were allowed to move freely in all spatial directions to allow for possible rotations of the water molecule. The adsorption simulation was run for 10 ps for each grid point, and the final E_{ads} (Eq. 1) was obtained by averaging the values of E_{ads} of the last 2.5 ps. The charge equilibration was performed every timestep.

Table 1. Density ρ and T_g of the simulated glasses.

x (mol %)	ρ (g/cm^3)	T_g (K)
5	2.74	1800
10	2.77	1780
15	2.81	1752

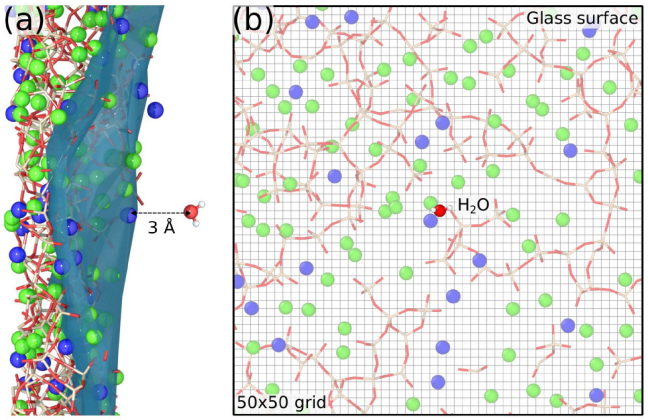

Figure 1. (a) A slice showing the distance between the water molecule and the glass surface. (b) shows a schematic representation of the calculation of the water adsorption energy.

Results

Bulk Glass Structure

The structure of the glass is validated in the paper that provided the parameter of the potential against many simulated binary and ternary silicate and aluminosilicate glasses.[23] The results showed very good agreement of the density and the structure obtained from this potential and experiments.[23] The structure factors $S(q)$ of all the simulated samples are plotted in Figure 2 along with the structure factor obtained by neutron diffraction experiments for the $(SiO_2)_{73.36}$-$(CaO)_{11.78}$-$(Na_2O)_{14.86}$ compositions taken from Ref. [39], which is the nearest composition to the simulated ones found in the literature. The structure factor obtained from the simulated glasses compares well to those obtained by neutron diffraction, which highlights the ability of the used interatomic potential in simulating glass models with realistic structures. Moreover, the position of the first sharp diffraction peak (FSDP) shifts towards larger q values, and its intensity decreases. The overall shape and trend of $S(q)$ obtained from experiments are well reproduced in the MD-simulated glass structures. An important observation obtained from the structure factors is that the short-ranged structure (large q values) is not affected by the composition. This is, in fact, observed in the pair distribution functions. In Figure 3(a), the first peak of the Si–O g(r) is shown for all glasses. The position of the first peak is not affected by the composition change and is centered around 1.58 Å, which is in good agreement with the data reported in the literature.[40–43] Similarly to the Si–O g(r), the coordination number of Si calculated by integrating the Si–O g(r) up to its first minimum (1.9 Å), did not show any change with changing the glass composition (See Table 2).

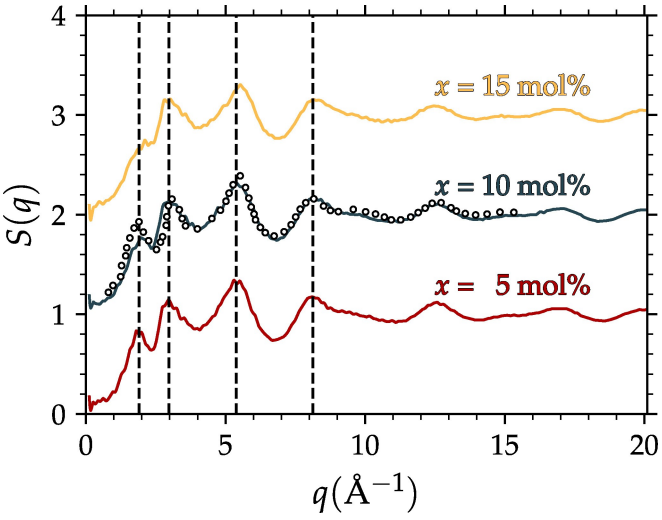

Figure 2. The structure factor for the simulated soda-lime silicate glasses (solid lines) compared to experimental structure factor from Cormier *et al.*[39] obtained by neutron diffraction of same or very close compositions (open circles). The labels for the simulated $S(q)$ are given in terms of Na_2O content, while for the experimental one, the composition is $(SiO_2)_{73.36}$-$(CaO)_{11.78}$-$(Na_2O)_{14.86}$. The vertical dashed lines highlight the position of the first four peaks in the $(SiO_2)_{60}$-$(CaO)_{35}$-$(Na_2O)_5$. It should be noted that the plots are shifted by one along the y-axis for clarity.

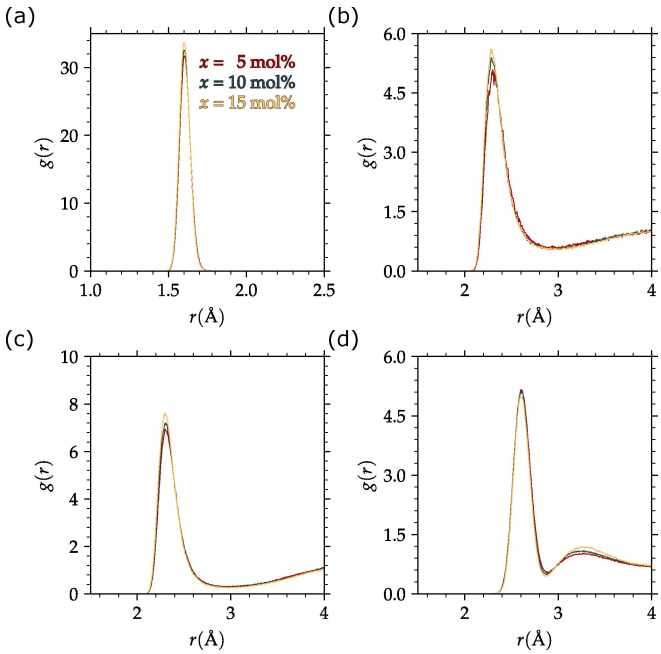

Figure 3. pair distribution function for (a) Si–O, (b) Na–O, (c) Ca–O, and (d) O–O in the bulk glasses at 300 K.

Table 2. Short-range structural parameters of glasses obtained from molecular dynamics at 300 K. The cutoffs were set to 2.0, 2.75, 2.8, and 2.9 Å for Si–O, Na–O, Ca–O, and O–O pairs, respectively.

	Si–O		Na–O		Ca–O		O–O	
x (mol %)	r_{ij}	N_{ij}	r_{ij}	N_{ij}	r_{ij}	N_{ij}	r_{ij}	N_{ij}
5	1.58	4.00	2.21	5.49	2.23	5.85	2.53	4.71
10	1.58	4.00	2.20	5.45	2.23	5.86	2.53	4.45
15	1.58	4.00	2.20	5.54	2.22	5.84	2.53	4.17

Figure 3(b and c) shows the change of the Na–O and Ca–O g(r) with increasing sodium content. With the increase of Na_2O at the expense of SiO_2, no visible change in the g(r) of both Na–O and Ca–O is observed. The bond length of Na–O was found to be 2.2 Å, and the of Ca–O is 2.23 Å. The mean coordination numbers of the Na–O and Ca–O pair are around 5.5 and 5.85, which were calculated up to the first minimum of the Na–O and Ca–O g(r) ($r_{min} = 2.75$ for Na–O and 2.8 for Ca–O).

The g(r) of the O–O are depicted in Figure 3(d) and show the mean distance between two oxygen atoms given by the position of its first peak. With the increase of Na_2O content, the O–O distance did not change on average. Further analysis of the oxygen local environment is characterized by the number of silicon atoms found in the first coordination shell of the oxygen. This enables the classification of oxygen atoms into different types, namely free oxygen (FO), non-bridging oxygen (NBO), and bridging oxygen (BO). Those are oxygen atoms that have 0, 1, or 2 Si atoms in the first coordination shell. The statistics of FO, NBO, and BO are shown in Figure 5, which shows the number of FO and NBO is increasing with increasing Na_2O content at the expense of decreasing BO content. This is expected as the content of the modifiers is increasing.

The angle distribution function (ADF) shown in Figure 4 indicates that the silicon atoms are forming tetrahedra (Figure 4(a) mean $\theta_{O-Si-O} \approx 109°$). The Si–O–Si bond angle distributions are presented in Figure 4(b) and provide information on the linkage between the SiO_4 tetrahedra. The Si–O–Si bond angle has a mean value around 135° and slightly changes to 130° values. On the other hand, for the O–Na–O and O–Ca–O angle distributions, the main peak is located at around 86° and a subpeak around 62° angles.

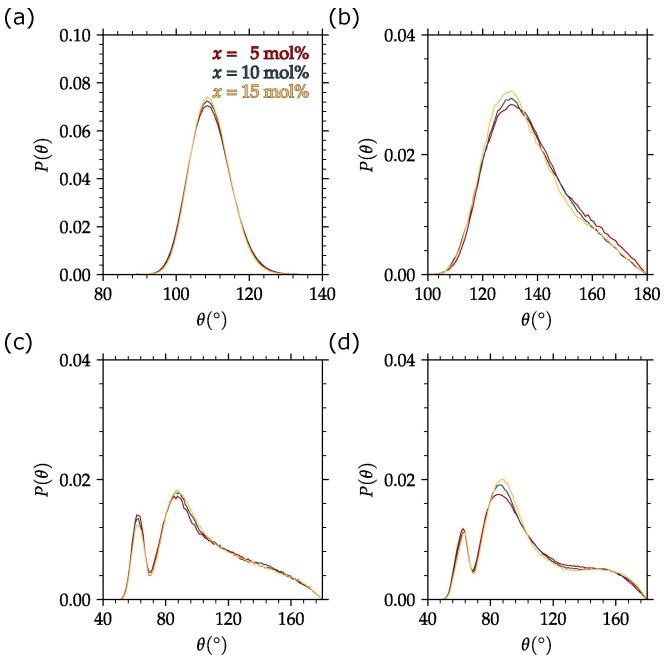

Figure 4. Bond angle distributions obtained of (a) O–Si–O, (b) Si–O–Si, (c) O–Na–O, and (d) O–Ca–O in the simulated glasses at 300 K.

The Q^n distribution can be used to get some insights on the near medium-range order in these glasses and how it changes with increasing Na_2O content. The n indicates the number of bridging oxygen in each silicon tetrahedra. Figure 6 shows histograms of the change of the Q^n species with composition. With the increase of Na_2O content, there is an increase in the low n Q^n ($n = 0$, 1, and 2), and there is a decrease of the high n Q^n ($n = 3$ and 4). This is in good agreement with the NBO and BO population analysis.

$$NC = \sum_{n=0}^{n} n x_n \tag{2}$$

The network connectivity of the glasses was calculated based on the Q^n distributions using Eq. 2 with x_n being the fraction of the Q^n, shown in Figure 6. The NC decreases with increasing Na_2O content. The NC of all glasses is below 3, which is suggested as a structural threshold for accessing the

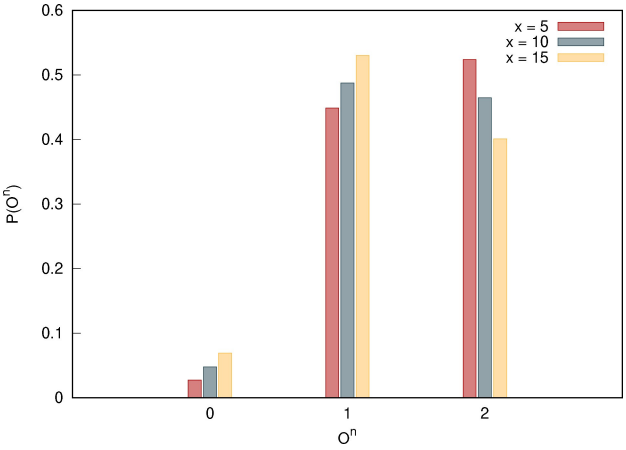

Figure 5. Histograms of the free oxygen O^0, non-bridging oxygen O^1, and bridging oxygen O^2 distribution in the soda-lime silicate glasses obtained from MD simulations at 300 K. The error is smaller than the symbol size.

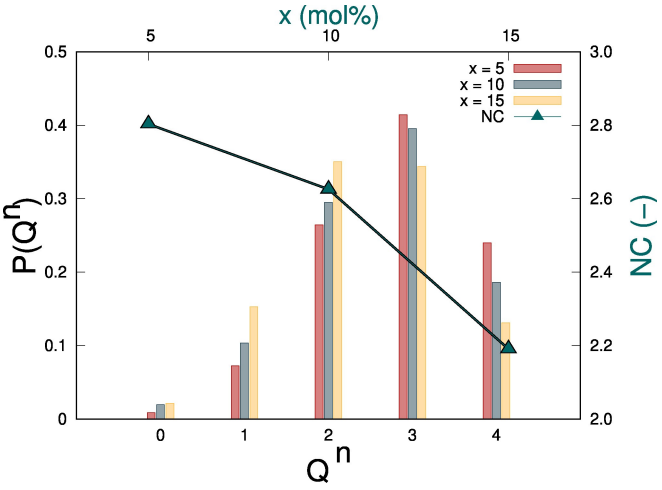

Figure 6. Histograms of the Q^n distribution of the silicon atoms in the soda-lime silicate glasses obtained from MD simulations at 300 K. On the secondary axes, the network connectivity (NC) of the same glasses is plotted as a function of the Na_2O content. The error is smaller than the symbol size.

bioactivity of the oxide glasses, meaning that all glasses are supposed to be bioactive.[14]

Glass Surface Structure

Although, the bioactivity of the glasses is often accessed using bulk dynamical properties and structure.[14–16] The first interaction of the glass with any physiological environment, e.g., soft tissues, is through its surface. Moreover, the surface plays an important role in determining the chemical durability of glasses. Thus, there is a need to also analyze the structure of the surface with the glass composition and its resemblance to the bulk structure and how it can be linked to the bioactivity and degradation behavior of the glasses.

The NBO and BO profiles shown in Figure 7(a and b) highlight that the oxygen atoms found at the surface are all NBOs, while they converge to the mean value in the bulk region (See Figure 5). On the other hand, the network connectivity shown in Figure 7(c) indicates that the glass surface is less connected than the bulk glass, which potentially will allow easier adsorption of water molecules in the interior of the glass. All results shown in Figure 7 confirmed that the surface is rich in Na and Ca (See Figure 10), and the first atomic layer at the surface is exclusively composed of NBO, Na, and Ca ions for all glasses.

On the other hand, the topological constraints of oxide glass surface were shown to be linked to the glass reactivity, such as dissolution rate and hydrophobicity.[20,44–46] Thus, in Figure 8, the topological constraints per atom maps of the glass surfaces are shown. The topological constraints were counted by excluding all NBOs, sodium, and calcium atoms from the structure. The number of rigid constraints n_c around each network-forming atom was then calculated using the eq. 3:

$$n_c = 2r - 3 + \frac{r}{2}, \tag{3}$$

where r is the average coordination number of network-forming atoms. This algorithm of counting the number of constraints is well established in the literature.[20,44–46] The surface was identified using a surface mesh with a probe sphere radius of 4.9 Å, and atoms that are 5 Å below the surface were considered to obtain the surface maps.

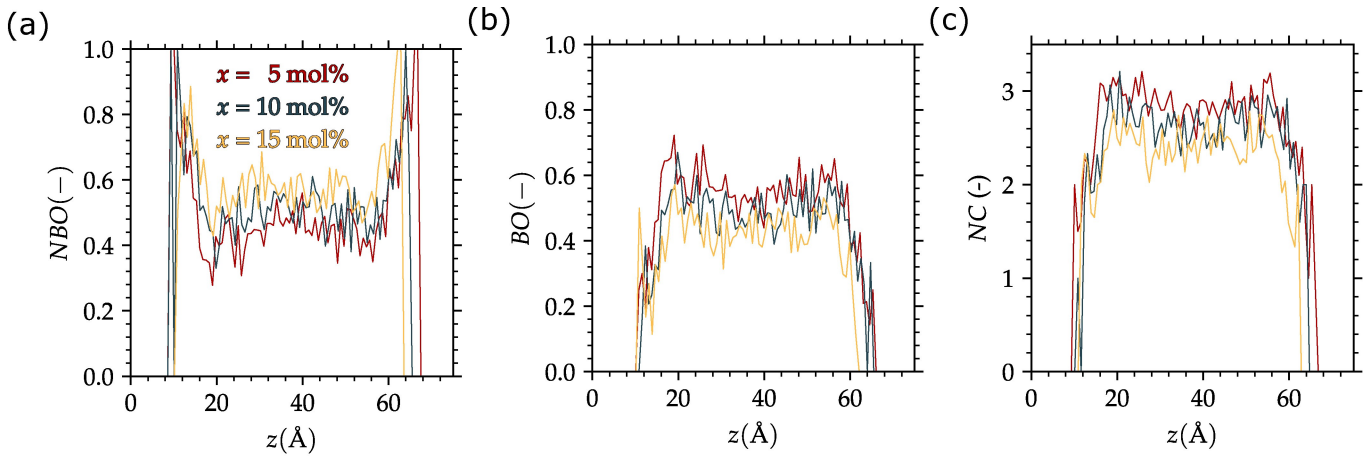

Figure 7. Profiles of (a) NBO concentrations, (b) BO concentrations, and (c) network connectivity along the *z*-axis, which is the surface normal axis.

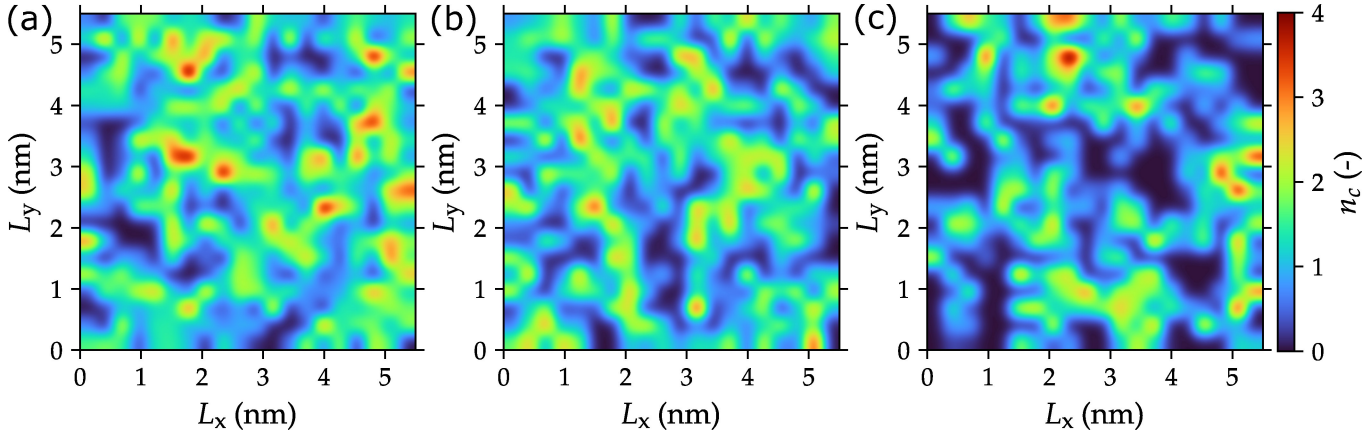

Figure 8. Topological constraints maps of the surfaces of the three glasses simulated in this work. The n_c data is averaged over 100 configurations, each separated by 1 ps. (a) is for $(SiO_2)_{60}(CaO)_{35}(Na_2O)_5$, (b) $(SiO_2)_{55\text{-}x}(CaO)_{35}(Na_2O)_{10}$, and (c) $(SiO_2)_{50}(CaO)_{35}(Na_2O)_{15}$.

It is clear from the surface constraints maps that the glasses go from a surface structure that is stresses-rigid ($n_c > 3$) to a flexible one ($n_c < 3$) with increasing Na_2O content. This transition is also linked to the increase of the Na and Ca on the surface compared to the bulk glasses. This indeed has implications on the dissolution rate and the surface hydrophilicity of the glasses, as the number of constraints per atom was shown to be a good descriptor to predict the dissolution rate and surface hydrophilicity,[19,20,47 48] where glasses that have lower surface constraints tend to be hydrophilic.[19,20]

Adsorption of H_2O on the Glass Surface

The adsorption energies were calculated using the method described in Sec. II. The results of the local adsorption energies are shown as a 2D heatmap in Figure 9 for all glasses. It should be noted that only the top surface was used for the calculations. In the top panels of Figure 9, histograms of the distribution of the local adsorption energies are shown, with the mean values μ and skewness *S* given inside each plot. In the top panel of Figure 9(c), a snapshot of a configuration with an adsorption energy of around −3 eV is shown. In this configuration, the water molecule is electrostatically attracted to the Na and Ca cations, with the distance between the oxygen from water and the nearby Na and Ca is nearly similar and is around 2.62 Å, which increases the binding strength of the water to the surface. Most of the E_{ads} values are between −3 and 0 eV. Although there are only very few studies similar to the current one, the current results are similar to the literature data for other silicate glasses.[18,20,49]

The mean value of adsorption energy decreases (increases in absolute values) with increasing Na_2O content. The decrease of the adsorption energies with Na_2O is because the content of the modifier on the surface increased, especially Na (See Figure 10). It should be noted that the values of the adsorption energies might be higher than the real ones, although a good agreement is observed when compared to other MD simulations, which is attributed to the fact that the glass further relaxes during the water adsorption simulations.

Discussion

The bulk and surface structures of soda-lime silicate glasses were investigated. The surfaces simulated in this work were intended to represent those of a real melt-quenched surface created during cooling, which is believed to be a realistic approach to modeling glass surfaces. The surface is richer in modifiers and NBOs than the bulk glass, which led to a decrease in its network connectivity (See Figure 7(b)). These changes in surface chemistry have implications for the surface structure and other properties it affects, such as bioactivity and degradation rate.

The adsorption of water on the surface of the glass plays a crucial role in determining the bioactivity of the glass, in particular in the formation of the HCA layer, which is necessary for bonding with biological tissues. The increase of Na and Ca density on the surface, as shown in Figure 10, leads to higher surface reactivity. This reactivity is reflected in the adsorption energies of water on the glass surface, where the adsorption energy was observed to increase, in absolute values, with the

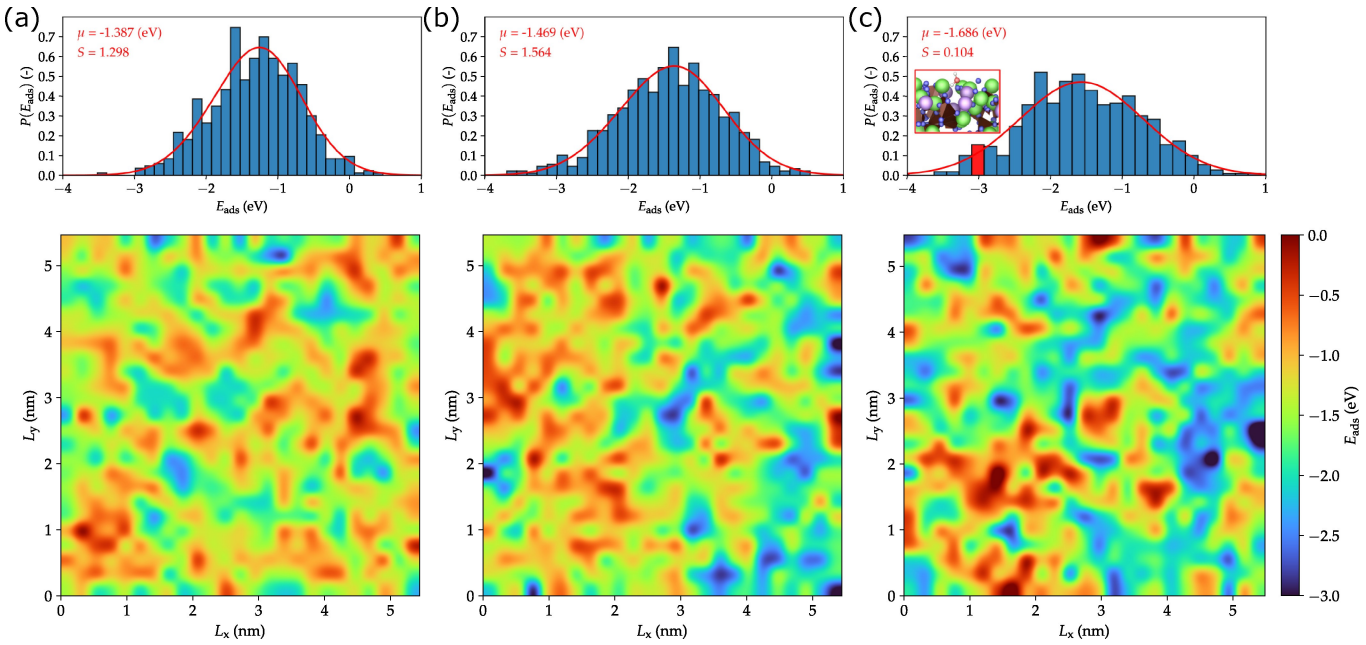

Figure 9. Top panels are histograms of the adsorption energy in the three glasses simulated in this paper (mean μ and skewness *S* are given inside each plot), while bottom panels are spatial maps of the Adsorption energy maps after having been coarse-grained through a Gaussian filter. (a) is for $(SiO_2)_{60}(CaO)_{35}(Na_2O)_5$, (b) $(SiO_2)_{55\text{-}x}(CaO)_{35}(Na_2O)_{10}$, and (c) $(SiO_2)_{50}(CaO)_{35}(Na_2O)_{15}$. In the top panel of (c) a snapshot of the atomic configuration at the adsorption energy of −3 eV is highlighted by the red box. The Si, Na, Ca, O glass, O water, and H are represented by brown tetrahedra, purple spheres, green spheres, blue spheres, red spheres, and white spheres, respectively.

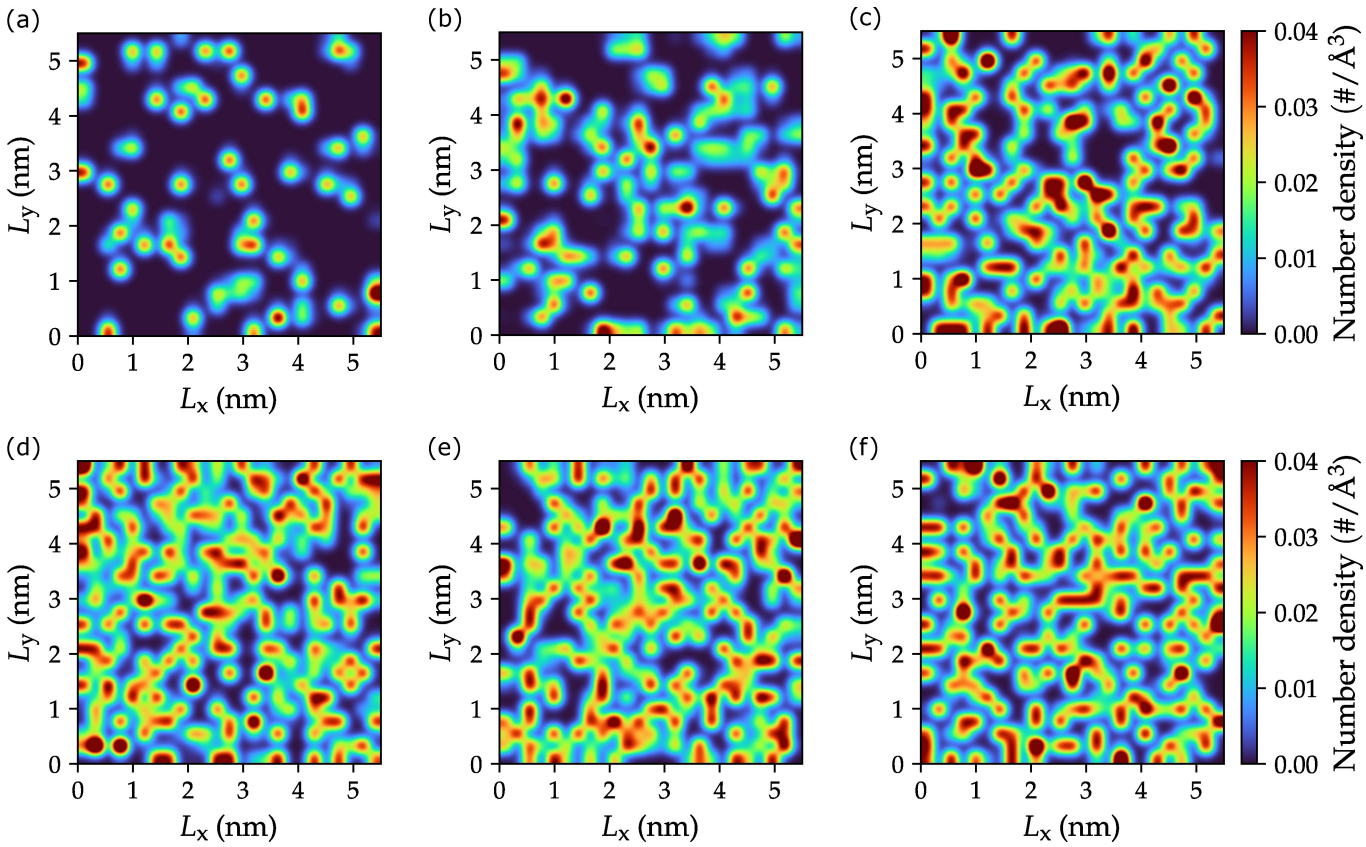

Figure 10. Top panels (a-c) are number density maps of Na atoms on the top surface, and bottom panels (d-f) are number density maps of Ca atoms on the top surface. (a and d) is for $(SiO_2)_{60}(CaO)_{35}(Na_2O)_5$, (b and e) $(SiO_2)_{55-x}(CaO)_{35}(Na_2O)_{10}$, and (c and f) $(SiO_2)_{50}(CaO)_{35}(Na_2O)_{15}$. All atoms within 5 Å from the surface are used to get the density maps. The data is averaged over 100 configurations, each separated by 1 ps.

increase of the density of the modifiers on the surface, leading to a stronger bonding on the surface. This promotes the formation of silanol groups (Si–OH^-), which increases the hydrophilicity of the surface, leading to an enhancement of its bioactivity. The creation of Si–OH^- groups is usually a precursor for the formation of the calcium phosphate layer (with phosphorus attracted from the physiological environments), which results in the precipitation and subsequent crystallization of HCA.

By comparing the results from the present simulations to other MD simulations using ReaxFF on sodium silicate glass, which highlighted the presence of a transition from what Wilkinson *et al.*[20] called a near hydrophilic–hydrophobic transition of the surface in the region around $n_c = 3.0$ constraints/atom. This was attributed to the isostatic nature of that region of the surface. However, this seems system-specific, as this transition was not observed in the current studied glasses. While the values of the E_{ads} shown in Figure 9 indeed depend on the local number of topological constraints per atom, no hydrophilic–hydrophobic transition can be reported. This behavior is explained by the fact that the surface of the glasses is rich in defects (e.g., NBO) and modifiers (Na and Ca), which favor water adsorption and binding, making the surface hydrophilic. This explanation is supported by the atomic density of Na and Ca cations depicted in Figure 10. This density was measured in the number of Na or Ca atoms/Å^3 and was calculated considering a surface thickness of 5 Å. The atomic density maps reveal that with increasing Na_2O content, the surface concentration of Na rises while that of Ca remains relatively constant. Consequently, modifier ions at the surface are anticipated to exhibit higher Lewis acidity than those within the bulk, rendering them highly reactive in physiological environments.[50,51] Moreover, if the surface is hydrophobic, the water molecules adsorbed on it are weakly attracted by the surface, and they are easily replaced by the hydroxyl groups.[52,53] On the contrary, if the surface is hydrophilic, the water molecules are strongly adsorbed on the hydroxyl groups, which have a higher degree of electron bond polarization with respect to oxygen ions within the glass matrix.[52,53] This will lead to a more sustained ion release, which also depends on the type of modifiers in the glass.[54]

It was shown that the presence of silicon linked by BO on the surface of the glass leads to hydrophobicity, which agrees with our observed results as more NBO were on the surface than BO.[17] As the Si–BO content decreases, the adsorption energy decreases (increases in absolute values), indicating that the adsorption becomes more favorable. Moreover, we found that the average adsorption energy in the Ca sites is always higher than that of the Na sites (See Table 3). However, the difference between the average adsorption energy in the Na

Table 3. Average adsorption energies in the Na sites $E_{ads,Na}$ and in the Ca sites $E_{ads,Ca}$, and the difference between these energies in (eV) at 300 K.

x (mol %)	$E_{ads,Na}$	$E_{ads,Ca}$	$E_{ads,Na} - E_{ads,Ca}$
5	−1.31	−1.35	0.04
10	−1.45	−1.48	0.03
15	−1.54	−1.55	0.01

site and adsorption energy in the Ca site decreases with increasing Na_2O content, which is due to the increase of surface Na atoms with the increase of Na_2O content (See Figure 10). Other simulations using Car-Parinello MD on soda-lime borosilicate glass have shown a similar trend regarding the difference between the adsorption energies in the Na sites and Ca sites.[55] Although those calculations were performed for only one site each, they still support the findings of the current work. Thus, it can be concluded that the local composition of the surface plays a significant role in defining the adsorption behavior of water and potentially other molecules on the surface.[56]

The results of this work highlight that the locality of the changes in the adsorption energies of H_2O on the soda-lime silicate glass surfaces is a key to understanding the bioactivity of the glasses. Higher $|E_{ads}|$ are typically correlated with more reactive surfaces, which means that the formation of silanol and other subsequent reactions of the ions exchange are facilitated. This reactivity is essential for forming the HCA layer, which allows the glass to bond effectively with the bones. Understanding the link between the adsorption energy and the surface chemistry will eventually allow for enhancing their bioactivity through surface engineering, making them more suitable for biomedical applications. In particular, in environments where controlled degradation and sustained ion release are necessary for bone regeneration and repair.[57–59]

Conclusions

In conclusion, three soda-lime silicate glasses were studied using a combination of classical and reactive molecular dynamics simulations. The structure of the glass surface was extensively studied and compared to the bulk structure in terms of NBO and BO content, as well as the network connectivity and modifiers density. The local adsorption energies strongly depended on the surface structure and composition. With the increase of the modifiers in the glass surface and defects, the water can bind strongly on the surface, which is the reason for the hydrophilicity of the surface. Moreover, a correlation was observed between the local adsorption energies and the local topological constraints per atom. We hope that the insights provided in this paper into the relationship between surface chemistry and the adsorption energy of water on soda-lime silicate glasses surfaces will pave routes for tailoring the properties of oxide glasses through surface engineering and for the rational design of new glasses with adapted properties, e.g., bioactivity, for medical applications. In particular, for applications where controlled degradation and ion release are necessary.

Acknowledgements

The author acknowledges the discussion with Dr. Sergey Sukhomlinov and Yasser Bakhouch. The author gratefully acknowledges the Gauss Centre for Supercomputing e.V. (www.gauss-centre.eu) for funding this project by providing computing time through the John von Neumann Institute for Computing (NIC) on the GCS Supercomputer JUWELS at Jülich Supercomputing Centre (JSC). Open Access funding enabled and organized by Projekt DEAL.

Conflict of Interests

There are no conflicts to declare.

Data Availability Statement

The data that support the findings of this study are available from the corresponding author upon reasonable request.

Keywords: Bioactive Glasses · Soda-Lime Silicate · Glass Surface Reactivity · Adsorption Energy · Reactive Molecular Dynamics

[1] A. Shearer, M. Montazerian, J. C. Mauro, *J. Non-Cryst. Solids* **2023**, *608*, 122228.
[2] A. Shearer, M. Montazerian, J. J. Sly, R. G. Hill, J. C. Mauro, *Acta Biomater.* **2023**, *160*, 14–31.
[3] X. Huang, Y. Lou, Y. Duan, H. Liu, J. Tian, Y. Shen, X. Wei, *Bioactive Materials* **2024**, *33*, 129–156.
[4] G. Kaur, O. Pandey, K. Singh, D. Homa, B. Scott, G. Pickrell, *J. Biomed. Mater. Res. Part A* **2013**, *102*, 254–274.
[5] O. D. Abodunrin, K. El Mabrouk, M. Bricha, *J. Mater. Chem. B* **2023**, *11*, 955–973.
[6] A. Moeini, T. Hassanzadeh Chinijani, A. Malek Khachatourian, M. Vinicius Lia Fook, F. Baino, M. Montazerian, *Int. J. Appl. Glass Sci.* **2022**, *14*, 69–87.
[7] D. S. Brauer, *Angew. Chem. Int. Ed.* **2015**, *54*, 4160–4181.
[8] S. Ferraris, I. Corazzari, F. Turci, A. Cochis, L. Rimondini, E. Vernè, *ACS Biomater. Sci. Eng.* **2021**, *7*, 2309–2316.
[9] E. A. Leed, J. O. Sofo, C. G. Pantano, *Phys. Rev. B* **2005**, *72*, 10.1103/physrevb.72.155427.
[10] P. Kiefer, R. Balzer, J. Deubener, H. Behrens, T. Waurischk, S. Reinsch, R. Müller, *J. Non-Cryst. Solids* **2019**, *521*, 119480.
[11] Y. Guo, Y. Zhou, D. Jia, H. Tang, *Microporous Mesoporous Mater.* **2009**, *118*, 480–488.
[12] T. Kono, T. Sakae, H. Nakada, T. Kaneda, H. Okada, *Minerales* **2022**, *12*, 170.
[13] F. Baino, S. Hamzehlou, S. Kargozar, *J, Funct. Biomater.* **2018**, *9*, 25.
[14] A. Atila, Y. Ouldhnini, S. Ouaskit, A. Hasnaoui, *Phys. Rev. B* **2022**, *105*, 10.1103/physrevb.105.134101.
[15] Y. Ouldhnini, A. Atila, S. Ouaskit, A. Hasnaoui, *Phys. Chem. Chem. Phys.* **2021**, *23*, 15292.
[16] Y. Ouldhnini, A. Atila, S. Ouaskit, A. Hasnaoui, *J. Non-Cryst. Solids* **2022**, *590*, 121665.
[17] V. A. Bakaev, W. A. Steele, *J. Chem. Phys.* **1999**, *111*, 9803–9812.
[18] E. A. Leed, C. G. Pantano, *J. Non-Cryst. Solids* **2003**, *325*, 48–60.
[19] Y. Yu, N. M. A. Krishnan, M. M. Smedskjaer, G. Sant, M. Bauchy, *J. Chem. Phys.* **2018**, *148*, 10.1063/1.5010934.

[20] C. J. Wilkinson, K. Doss, S. H. Hahn, N. Keilbart, A. R. Potter, N. J. Smith, I. Dabo, A. C. T. van Duin, S. H. Kim, J. C. Mauro, *J. Phys. Chem. Lett.* **2019**, *10*, 3955–3960.
[21] E. Kilinc, R. J. Hand, *J. Non-Cryst. Solids* **2015**, *429*, 190–197.
[22] L. L. Hench, R. J. Splinter, W. C. Allen, T. K. Greenlee, *J. Biomed. Mater. Res.* **1971**, *5*, 117–141.
[23] S. Sundararaman, L. Huang, S. Ispas, W. Kob, *J. Chem. Phys.* **2019**, *150*, 10.1063/1.5079663.
[24] C. J. Fennell, J. D. Gezelter, *J. Chem. Phys.* **2006**, *124*, 234104.
[25] A. Atila, E. Bitzek, *J. Non-Cryst. Solids* **2024**, *627*, 122822.
[26] Z. Pan, A. Atila, E. Bitzek, L. Wondraczek, *J. Non-Cryst. Solids* **2024**, *627*, 122801.
[27] Y. Bakhouch, S. Buchner, R. A. Silveira, L. Resende, A. S. Pereira, A. Hasnaoui, A. Atila, *J. Am. Ceram. Soc.* **2024**, 10.1111/jace.19778.
[28] S. Ganisetti, A. Atila, J. Guénolé, A. Prakash, J. Horbach, L. Wondraczek, E. Bitzek, *Acta Mater.* **2023**, *257*, 119108.
[29] A. Atila, E. M. Ghardi, A. Hasnaoui, S. Ouaskit, *J. Non-Cryst. Solids* **2019**, *525*, 119470.
[30] A. Atila, E. M. Ghardi, S. Ouaskit, A. Hasnaoui, *Phys. Rev. B* **2019**, *100*, 10.1103/physrevb.100.144109.
[31] H. Kharouji, A. Hasnaoui, A. Atila, *Materia* **2024**, *36*, 102148.
[32] A. P. Thompson, H. M. Aktulga, R. Berger, D. S. Bolintineanu, W. M. Brown, P. S. Crozier, P. J. in 't Veld, A. Kohlmeyer, S. G. Moore, T. D. Nguyen, R. Shan, M. J. Stevens, J. Tranchida, C. Trott, S. J. Plimpton, *Comput. Phys. Commun.* **2022**, *271*, 108171.
[33] A. Stukowski, *Model. Simul. Mater. Sci. Eng.* **2010**, *18*, 015012.
[34] A. C. T. van Duin, S. Dasgupta, F. Lorant, W. A. Goddard, *J. Phys. Chem. A* **2001**, *105*, 9396–9409.
[35] T. P. Senftle, S. Hong, M. M. Islam, S. B. Kylasa, Y. Zheng, Y. K. Shin, C. Junkermeier, R. Engel-Herbert, M. J. Janik, H. M. Aktulga, T. Verstraelen, A. Grama, A. C. T. van Duin, *npj Comput. Mater.* **2016**, *2*, 10.1038/npjcompumats.2015.11.
[36] A. K. Rappe, W. A. Goddard, *J. Phys. Chem.* **1991**, *95*, 3358–3363.
[37] A. Nakano, *Comput. Phys. Commun.* **1997**, *104*, 59–69.
[38] H. Aktulga, J. Fogarty, S. Pandit, A. Grama, *Parallel Comput.* **2012**, *38*, 245–259.
[39] L. Cormier, G. Calas, B. Beuneu, *J. Non-Cryst. Solids* **2011**, *357*, 926–931.
[40] C. Karlsson, E. Zanghellini, J. Swenson, B. Roling, D. T. Bowron, L. Börjesson, *Phys. Rev. B* **2005**, *72*, 10.1103/physrevb.72.064206.
[41] O. Laurent, B. Mantisi, M. Micoulaut, *J. Phys. Chem. B* **2014**, *118*, 12750–12762.
[42] S. Locker, J. A. Clark, S. Sundaram, *Int. J. Appl. Glass Sci.* **2020**, *12*, 25–35.
[43] J. F. S. Christensen, S. S. Sørensen, T. To, M. Bauchy, and M. M. Smedskjaer, *Phys. Rev. Mater.* **2021**, *5*, 10.1103/physrevmaterials.5.093602
[44] J. C. Mauro et al, *Am. Ceram. Soc. Bull.* **2011**, *90*, 31.
[45] M. Bauchy, M. J. Abdolhosseini Qomi, C. Bichara, F.-J. Ulm, R. J.-M. Pellenq, *J. Phys. Chem. C* **2014**, *118*, 12485–12493.
[46] T. Oey, E. C. La Plante, G. Falzone, K. Yang, A. Wada, M. Bauchy, J. W. Bullard, G. Sant, *J. Am. Ceram. Soc.* **2020**, *103*, 6198–6207.
[47] M. Bauchy, *Comput. Mater. Sci.* **2019**, *159*, 95–102.
[48] I. Pignatelli, A. Kumar, M. Bauchy, G. Sant, *Langmuir* **2016**, *32*, 4434–4439.
[49] A. C. Antony, S. Goyal, H. Park, J. Banerjee, N. J. Smith, G. Agnello, R. G. Manley, *J. Phys. Chem. B* **2022**, *126*, 7709–7719.
[50] A. Pedone, V. Cannillo, M. C. Menziani, *Acta Mater.* **2021**, *213*, 116977.
[51] P. Sahu, S. M. Ali, *Langmuir* **2022**, *38*, 7639–7663.
[52] S. Ferraris, S. Yamaguchi, N. Barbani, M. Cazzola, C. Cristallini, M. Miola, E. Vernè, S. Spriano, *Acta Biomater.* **2020**, *102*, 468–480.
[53] R. Mathew, C. Turdean-Ionescu, Y. Yu, B. Stevensson, I. Izquierdo-Barba, A. García, D. Arcos, M. Vallet-Regí, M. Edén, *J. Phys. Chem. C* **2017**, *121*, 13223–13238.
[54] A. Atila, S. Ouaskit, A. Hasnaoui, *Phys. Chem. Chem. Phys.* **2020**, *22*, 17205.
[55] H. Jabraoui, T. Charpentier, S. Gin, J.-M. Delaye, R. Pollet, *J. Chem. Phys.* **2022**, *156*, 10.1063/5.0087390.
[56] B. Siboulet, B. Coasne, J.-F. Dufrêche, P. Turq, *J. Phys. Chem. B* **2011**, *115*, 7881–7886.
[57] Y. Zhu, X. Zhang, G. Chang, S. Deng, H. F. Chan, *Adv. Mater.* **2024**, 10.1002/adma.202312964.
[58] G. Duan, D. Chang, C. Zhang, S. Li, X. Liu, Z. Wang, L. Chen, J. Li, Z. Bai, J. Weng, *Biosurface Biotribology* **2024**, *10*, 17–41.
[59] P. A. Dash, S. Mohanty, S. K. Nayak, *J. Non-Cryst. Solids* **2023**, *614*, 122404.

Manuscript received: March 31, 2024
Revised manuscript received: September 3, 2024
Accepted manuscript online: September 4, 2024
Version of record online: November 3, 2024